GEOPHYSICAL RESEARCH LETTERS
October 2006; 33 : L06609
http://dx.doi.org/10.1029/2005GL024938

Salinity changes along the upper limb of the Atlantic thermohaline circulation

Bruno Blanke[a*], Michel Arhan[b], Sabrina Speich[a]

[a]Laboratoire de Physique des Océans, UFR Sciences et Techniques, 6 avenue Le Gorgeu - C.S. 93837, F-29238 Brest Cedex 3, France.
[b]Laboratoire de Physique des Océans, IFREMER/Centre de Brest, BP 70, F-29280 Plouzané, France.

*: Corresponding author : blanke@univ-brest.fr

Abstract: Lagrangian analyses of a global ocean circulation model quantify the salinity changes experienced by the warm limb of the thermohaline circulation during the northward flow to the Atlantic deep convection regions. 6 Sv out of the estimated 10-Sv transfer from 45°S to 47°N flow through regions of prevailing surface evaporation: the southern and northern formation regions of Salinity Maximum Water and the Gulf of Cadiz/Mediterranean Sea domain. The remaining transport gains salinity through mixing with adjacent waters. As much as 6 Sv flow through the low-salinity surface mixed layer at the latitudes of the ITCZ whose effect annihilates that of the southern region of Salinity Maximum Water. Most of the salinity increase corresponds to the transformation of South to North Atlantic Central Water, with strong diapycnal transfers for the water that intersects the high and low salinity regions, and nearly isopycnal modifications for the water that avoids these regions.

1. Introduction

The high salinity values of the upper North Atlantic are a precondition for deep convection in the northern part of this basin and in the Arctic Seas. Deep convection is a key process of the global thermohaline circulation (THC), and most climate models predict a weakening of the THC under the effect of human-induced global warming and subsequent surface salinity decrease at high latitudes [Manabe and Stouffer, 1993; Gregory et al., 2005]. There is, however, much uncertainty on the predicted amplitude of the weakening, and some experiments even suggest that increased salinity transfers from the tropics can offset this first response [Latif et al., 2000; Thorpe et al., 2001]. These uncertainties emphasize the need for refined descriptions of the meridional evolution of salinity in the warm limb of the THC, which constitute a prerequisite to a better understanding of the chain of processes responsible for relatively high salinities at the entry of the northern convective regions.

Gordon and Piola [1983] evidenced a two-bump distribution in the Atlantic meridional salinity variations with maxima around 17°S and 25°N where a prevalence of evaporation over precipitation leads to the formation of Salinity Maximum Water (SMW) at the surface [Worthington, 1976]; they also found a local minimum at the latitudes of the Intertropical Convergence Zone (ITCZ) where intense precipitations and river runoffs cause a freshening of the surface waters. In the light of these observations, we use a global model in order to diagnose the main salinity changes undergone by the northward flowing warm limb water throughout the Atlantic. We analyze the mass transport achieved from the southern South Atlantic to the edge of the northern convection region from a Lagrangian analysis of the simulated velocity fields. As this analysis implicitly diagnoses mixing, we evaluate water mass conversions and overall salinity and density changes along the northward progress. Finally, we estimate the relative importance of the two SMW formation regions and the Mediterranean domain as regions of salinity increase as well as the counteracting effect of the ITCZ latitudes.

2. Model Description

We analyze the last year of a 10-year simulation of the global OPA (Océan Parallélisé) model [Madec et al., 1998] coupled with the Louvain-La-Neuve ice model [Fichefet and Morales Maqueda, 1997]. The ocean model has 0.5° horizontal resolution and 30 levels. Bottom topography and coastlines are from Smith and Sandwell [1997] complemented by the ETOPO5 data set, and bottom stress is determined by using a quadratic drag law. Vertical eddy viscosity and diffusivity coefficients are computed using a 1.5 turbulent closure scheme, and double diffusion is parameterized with distinct coefficients for temperature and salinity [Merryfield et al., 1999]. Lateral mixing on dynamics is horizontal; it is supplemented with the Gent and McWilliams [1990] eddy-induced velocity parameterization with a coefficient depending on the growth rate of baroclinic instability [Guilyardi et al., 2001]. Lateral mixing of heat and salt occurs only along neutral surfaces. The model is forced by a daily climatology derived from the weekly ERS[1] 10-year (1992–2001) wind stress and completed by the daily NCEP[2] climatology poleward of 50°. Surface heat fluxes and evaporation are computed with bulk formulas including climatologies for surface air temperature, specific humidity and cloud cover. The surface freshwater flux is derived from CMAP[3] precipitation maps and from the monthly runoff of the main rivers.

Surface fluxes use an additional relaxation to the surface temperature and salinity of Levitus et al. [1998] with a characteristic time scale that varies linearly with the depth of the surface mixed layer (11.5 days for 10 m). Another important characteristic of the simulation is a restoring term to the Levitus et al. [1998] climatology in the tracer equations. This Newtonian damping is added in the ocean interior, except in the 20°S-20°N latitude band and in the surface mixed layer to avoid interference with the model fast adjustment in these regions. The damping is also slightly relaxed poleward of 50°

[1] ERS: European Remote Sensing satellites.
[2] NCEP: National Centers for Environmental Prediction.
[3] CMAP: CPC (Climate Prediction Center) Merged Analysis of Precipitation

because of sparse observations and it comes progressively to zero within 1000 km of the coastlines because of a poor capture of boundary currents by climatologies. Its intensity is defined as the inverse of a timescale that varies from 50 days below the surface mixed layer to 360 days at 5000 m.

Our Lagrangian trajectory analysis builds on previous studies on the tropical and subtropical Atlantic [Blanke et al. 1999, 2002; Donners et al., 2005]. Computed trajectories are not aimed at simulating the motions of individual water parcels within the ocean; they rather represent three-dimensional streamlines within the monthly-archived large-scale velocity fields. These fields include the eddy-induced velocity computed with the Gent and McWilliams [1990] scheme and integrate the mean effect of turbulent mixing on the momentum equations as calculated by the ocean model with its parameterizations of sub-grid scale turbulence.

3. Results

The effect of the relaxation to the climatology [Levitus et al., 1998] was verified by comparing model meridional distributions at 30°W/35°W against available direct measurements at similar longitudes. Figure 1 shows the remote origins of the northward flowing transport at 47°N through a transport streamfunction built as in Blanke et al. [1999]. The amplitude of the transfer is 10 Sv. We stress that this is not the full northward transport at 47°N, but it corresponds only to the fraction related to a mass transfer from the southern South Atlantic (45°S or 19°E). This value also differs from the amplitude of the model meridional overturning (about 15 Sv at the equator) as the latter includes water conversion south of 47°N (mostly by convection in the Mediterranean Sea and by entrainment in the Gulf of Cadiz). These 10 Sv in the model almost exclusively correspond to water entering the Atlantic at its southeastern corner, with hardly any direct entrance of near-surface water from the Antarctic Circumpolar Current. The pathways across the Atlantic show only a weak recirculation in the southern subtropical gyre, a stronger recirculation associated with the Subtropical Cells [Malanotte-Rizzoli et al., 2000] in the equatorial region, and a transmission to 47°N by the North Brazil Current, the Gulf Stream and eventually the North Atlantic Drift, with an intense recirculation in the northern subtropical gyre.

Salinity increase in the course of the northward water transfer may occur either directly through a temporary transit in a region of high salinity gained by an excess of evaporation over precipitation, or indirectly through mixing with more saline adjacent water. We note that the relaxation term to the climatology also induces property changes in areas where modeled tracers differ from observations. The thin lines in Figure 2 show the transport streamfunctions in the latitude-salinity and latitude-temperature domains. These diagrams are obtained in the same way as in Figure 1 except the projection and combination of individual particle transports along different sets of axes. In Figure 2a, three high salinity excursions in the streamlines correspond to three major regions of saline water formation. Two of them, around 13°S and 20°N, reveal the southern and northern SMW formation regions (S-SMW, N-SMW; see Fig. 1). The one near 35°N is not an absolute maximum, but is a peak for the streamlines that compose it and corresponds to the Gulf of Cadiz and Mediterranean Sea domains (GC/MS; see Fig. 1). To quantitatively determine the transits through these regions, S-SMW and N-SMW were defined as three-dimensional oceanic domains by using criteria on surface salinity (>36.6) and density (with a departure from surface values less than $\Delta\rho = 0.01$ kg/m^3). The GC/MS region was defined as the oceanic volume located east of 9°W (Fig. 1). With these definitions, the transits through S-SMW, N-SMW and GC/MS are 2.6, 4.9 and 2.4 Sv, respectively, whereas the transport associated with particles avoiding these regions is 3.6 Sv and consists of lower Central Water and Intermediate Water with an average density of 27 σ_0. Because the transits through the high salinity regions are not exclusive, the first three values overlap, and the transports add up to more than the net northward transfer of 10 Sv. We further defined the freshening oceanic domain around ITCZ latitudes (F-ITCZ; see Fig. 1) as the surface mixed layer ($\Delta\rho<0.01$ kg/m^3) of the region of surface salinity lower than 35.6

within the band 10°S-15°N. In the model, the transit through F-ITCZ is 6 Sv; this high percentage (60%) is probably explained by the location of this near-surface domain just downstream of the equatorial upwelling.

Let us now classify the particles according to the last high-salinity region they cross before reaching 47°N; the net transfer breaks down into 0.6 (S-SMW), 3.5 (N-SMW), 2.4 (GC/MS) and 3.6 Sv (no transit). The median streamlines associated with these groups are shown in Figure 2 by thick contours. A large overlap of the groups of particles passing across the different salinization areas is reflected in similar curves for the three regions. These curves also show that the salinity increase in the S-SMW region is annihilated in F-ITCZ. The model indicates that 96% of the volume transport through S-SMW subsequently intersect F-ITCZ; this result corroborates similar conclusions drawn by Donners et al. [2005] and explains the weak net contribution of S-SMW to the THC upper limb salinization. At variance with this behavior, we find that only 0.4 Sv of the 4.9 Sv flowing through N-SMW subsequently intersects F-ITCZ, which implies a more effective role of N-SMW in the net salinity increase. We note, however, that 1.4 Sv of the transport through N-SMW further intersects GC/MS.

On average, the particles subject to *direct* salinization experience a salinity increase of 0.38 psu across the Atlantic to 47°N; this elevation of salinity being associated with a net 2.5°C cooling (Fig. 2b) results in a density increase of 0.78 kg/m^3 before the particles reach the northern convective region. The water that does not flow through any high-salinity region experiences a slightly stronger net salinity increase (0.56), yet with a temperature increase (2.3°C); its density is only increased by 0.12 kg/m^3. Figure 2a shows that the latter fraction shows no significant modification prior to reaching 13°N-15°N where a first salinity jump of 0.4 occurs. These latitudes mark the transition between the South and North Atlantic Central Waters (SACW, NACW; Sverdrup et al. [1942]). Another sharp salinity gradient stands out just south of 39°N likely because of mixing with the Mediterranean outflow water [e.g., Needler and Heath, 1975]. To the north of this latitude, finally, the freshening northern influence affects all the components of the upper THC limb.

The researchers who study water mass properties frequently consider the Atlantic northward salinity increase as reflecting the conversion of SACW into NACW. The Cape Verde Front at 10°N-15°N across the Atlantic [Zenk et al., 1991] separates both varieties, the latter being about 1 psu saltier than the former along isopycnals. In order to examine how this conversion occurs, we project the northward mass transfer of warm water onto a salinity-temperature diagram. Figure 3 shows that the T-S patterns at 45°S-19°E and 47°N have nearly linear shapes typical of SACW and NACW with the addition of some Mediterranean Water at 47°N. Water conversions are represented by arrows on these parts of the diagram because these areas correspond to sources and sinks of mass in our T-S domain. A mass streamfunction can be defined anywhere else, and conversions are displayed with contours. Figure 3 highlights the two main T-S routes at the origin of the transformation of SACW into NACW. One of them (the 3.6 Sv avoiding the high salinity regions) transforms lower SACW and intermediate water into lower NACW along apparent isopycnal tracks. In the model, about 2.6 Sv of the transport along this route occur near the western boundary at 10°N-15°N, whereas the remaining 1 Sv flows through the ocean interior before merging with the former fraction in the Caribbean Sea. The mixing processes related to the western boundary path should, therefore, dominate the water conversion along this first route, and among them, notably those associated with the propagation and decay of North Brazil Current rings [Johns et al., 2003] and double-diffusion of lower SACW with overlying SMW [Schmitt et al., 1987]. The low density ratio associated with the latter mechanism unlikely alters the apparent isopycnic character of this transfer in Figure 3. Other mixing processes like intermingling across the Cape Verde Front and mechanisms related to eastern-boundary flows [Tomczak, 1981] should be associated with the 1 Sv flowing through the ocean interior. The other route from SACW to NACW (Fig. 3) is more complex and calls on intense temperature and salinity variations corresponding to transits through one or several of the three high salinity regions and the fresh domain at ITCZ latitudes. As expected from a direct exposure of the water to air-sea exchanges in these regions, the temperature-salinity changes along this route are strongly diapycnal. Vertical mixing and convection in the three domains, S-SMW, N-SMW and GC/MS, should naturally be the major salinization mechanisms along this second route.

4. Concluding remarks

We put at 4.4×10^{6} kg/s the net average enrichment rate in salt along the full transfer. The accumulation or withdrawal rates diagnosed locally after the waters have crossed the subtropical or equatorial regions are roughly four times larger than this net rate and can balance each other. For instance, the accumulation of salt in the surface and thermocline waters after passage in the S-SMW formation region almost entirely disappears past the equatorial region. However, a net positive rate is an unquestionable sign of the ability of the Atlantic domain to salinize waters in transit. Ongoing investigations are aimed at quantifying the impact of the relaxation to climatological tracer fields poleward of 20°. Such assessment is required for a better evaluation of the parts played by the various mixing processes along the routes described here, and for any meaningful comparison of the net salinization rate at 47°N with the air- and ice-sea exchanges in the northern subpolar and polar regions. The isopycnic propagation of temporal salinity anomalies between SMW formation regions and the Arctic Seas would also provide valuable information about mechanisms implicated in climate variability at decadal to centennial time scales.

Acknowledgments. BB, MA and SS acknowledge support from IFREMER and INSU/CNRS through the French Programme National d’Étude de la Dynamique du Climat. The authors wish to thank two anonymous reviewers for comments and suggestions and express their gratitude to Gurvan

Madec (leading the OPA modeling system) for fruitful discussions and Marie-Paule Friocourt for her assistance in correcting the manuscript.

5. References

Blanke B., M. Arhan, G. Madec, and S. Roche, Warm water paths in the equatorial Atlantic as diagnosed with a general circulation model, *J. Phys. Oceanogr.*, **29**, 2753-2768, 1999.

Blanke B., M. Arhan, A. Lazar, and G. Prévost, A Lagrangian numerical investigation of the origins and fates of the Salinity Maximum Water in the Atlantic, *J. Geophys. Res.*, **107**, 3163, doi:10.1029/2002JC001318, 2002.

Donners J., S.S. Drijfhout and W. Hazeleger, Water mass transformation in the South Atlantic, *J. Phys. Oceanogr.*, **35**, 1841-1860, 2005.

Fichefet, T., and M.A. Morales Maqueda, Sensitivity of a global sea ice model to the treatment of ice thermodynamics and dynamics, *J. Geophys. Res.*, **102**, 609-646, 1997.

Gent, P.R., and J.C. McWilliams, Isopycnal mixing in ocean circulation models, *J. Phys. Ocean.*, **20**, 150-155, 1990.

Gregory J.M., K.W. Dixon, R.J. Stouffer, A.J. Weaver, E. Driesschaert, M. Eby, T. Fichefet, H. Hasumi, A. Hu, J.H. Jungclaus, I.V. Kamenkovitch, A. Levermann, M. Montoya, S. Murakami, S. Nawrath, A. Oka, A.P. Sokolov, and R.B. Thorpe, A model intercomparison of changes in the Atlantic thermohaline circulation in response to increasing atmospheric CO_2 concentration, *Geophys. Res. Lett.*, **32**, L12703, doi:10.1029/2005GL023209, 2005.

Gordon, A.L., and A.R. Piola, Atlantic Ocean upper layer salinity budget, *J. Phys. Oceanogr.*, **13**, 1293-1300, 1983.

Guilyardi E., G. Madec, and L. Terray, The role of lateral ocean physics in the upper ocean thermal balance of a coupled ocean-atmosphere GCM, *Climate Dyn.*, **17**, 589-599, 2001.

Johns W.E., R.J. Zantopp and G.J. Goni, Cross-gyre transport by the North Brazil Current rings. In: Interhemispheric water exchange in the Atlantic Ocean, G.J. Goni and P. Malanotte-Rizzoli eds., Elsevier Oceanographic series, **68**, 411-441, 2003.

Latif M., E. Roeckner, U. Mikolajewicz, and R. Voss, Tropical stabilization of the thermohaline circulation in a greenhouse warming simulation, *J. Climate*, **13**, 1809-1813, 2000.

Levitus, S., R. Burgett, and R.P. Boyer, *Introduction*. Vol. 1, *World Ocean Database 1998*, NOAA Atlas NESDIS 18, 346 pp., 1998.

Madec, G., P. Delecluse, M. Imbard, and C. Lévy, OPA 8.1 Ocean General Circulation Model reference manual, *Notes du Pôle de Modélisation de l'Institut Pierre-Simon Laplace*, **11**, 91 pp., available from LODYC, Univ. Pierre et Marie Curie –Case 100, 4 place Jussieu, 75252 Paris Cedex 05, France, 1998.

Malanotte-Rizzoli P., K. Hedstrom, H. Arango, and D.B. Haidvogel, Water mass pathways between the subtropical and tropical ocean in a climatological simulation of the North Atlantic Ocean circulation, *Dyn. Atmos. Oceans*, **32**, 331-371, 2000.

Manabe, S, and R.J. Stouffer, Century-scale effects of increased atmospheric CO_2 on the ocean-atmosphere system, *Nature*, **364**, 215-218, 1993.

Merryfield, W.J., G. Holloway, and A.E. Gargett, A global ocean model with double-diffusive mixing. *J. Phys. Oceanogr.*, **29**, 1124-1142, 1999.

Needler G.T. and R.A. Heath, Diffusion coefficients calculated from the Mediterranean salinity anomaly in the North Atlantic Ocean, *J. Phys. Oceanogr.*, **5**, 173-182, 1975.

Schmitt R..W., H. Perkins, J.D. Boyd, M.C. Stalcup, C-Salt: An investigation of the thermohaline staircase in the western tropical North Atlantic, *Deep-Sea Res.*, **34**, 1655-1665, 1987.

Smith W.H.F., and D.T. Sandwell, Global sea floor topography from satellite altimetry and ship depth soundings, *Science*, **227**, 1956-1962, 1997.

Sverdrup H.U., M.W. Johnson and R.H. Fleming, The Oceans. Their physics, chemistry and general biology. Prentice-Hall, Englewood Cliffs, NJ, 1087 pp, 1942.

Thorpe, R.B., J.M. Gregory, T.C. Johns, R.A. Wood, and J.F.B. Mitchell, Mechanisms determining the Atlantic thermohaline circulation response to greenhouse gas forcing in a non-flux-adjusted coupled climate model, *J. Climate*, **14**, 3102-3116, 2001.

Tomczak M., An analysis of mixing in the frontal zone of South and North Atlantic Central Water off North-West Africa, *Prog. Oceanogr.*, **10**, 173-190, 1981.

Worthington, L.V., On the North Atlantic Circulation, *Johns Hopkins Oceanogr. Stud.*, **6**, 110 pp., Johns Hopkins Univ. Press, Baltimore, Md, 1976.

Zenk, W., B. Klein, and M. Schröder, Cape Verde frontal zone, *Deep-Sea Res.*, **38** (Suppl.), S505-S530, 1991.

Figure captions

Figure 1. Horizontal mass streamfunction related to the vertically-integrated transport of the northward transfer of warm water across the Atlantic. The contour interval is 1 Sv. The salinization regions discussed in the text are light-shaded, and the freshening oceanic domain around ITCZ latitudes is dark-shaded.

Figure 2. Projection of the warm water transfer. (a) Onto a salinity-latitude diagram. (b) Onto a temperature-latitude diagram. The contour interval is 1 Sv. Bold lines show the median contours obtained by limiting the transfer to: i) the waters that last intercept the N-SMW (long-dashed, light grey) or S-SMW formation regions (long-dashed, dark grey) or the GC/MS domain (dash-dotted), or to ii) the waters that avoid the three salinization regions (short-dashed). The approximate meridional extent of each of the three salinization regions is shaded on the left panel.

Figure 3. Projection of the warm water transfer onto a salinity-temperature diagram. For all particles, light- and dark-grey dots show the initial (45°S-19°E) and final (47°N) conditions, respectively. Schematic salinity and temperature ranges covered by the three salinization regions are shaded.

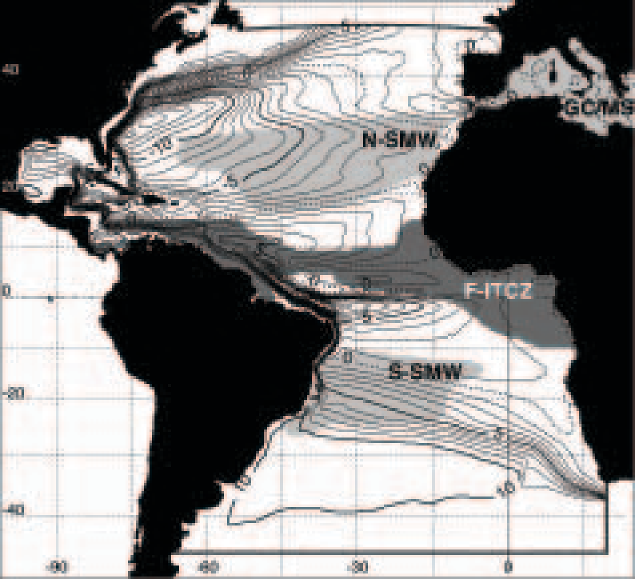

N-SMW
F-ITCZ
S-SMW
GC/MS
40
20
0
-20
-40
-90
-60
-30
0

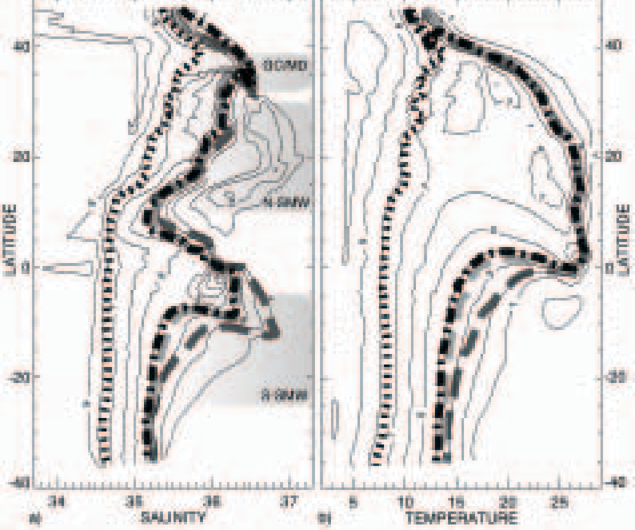

GO/MD
N-SMW
S-SMW
LATITUDE
40
20
0
-20
-40
34
35
36
37
a)
SALINITY
5
10
15
20
25
b)
TEMPERATURE

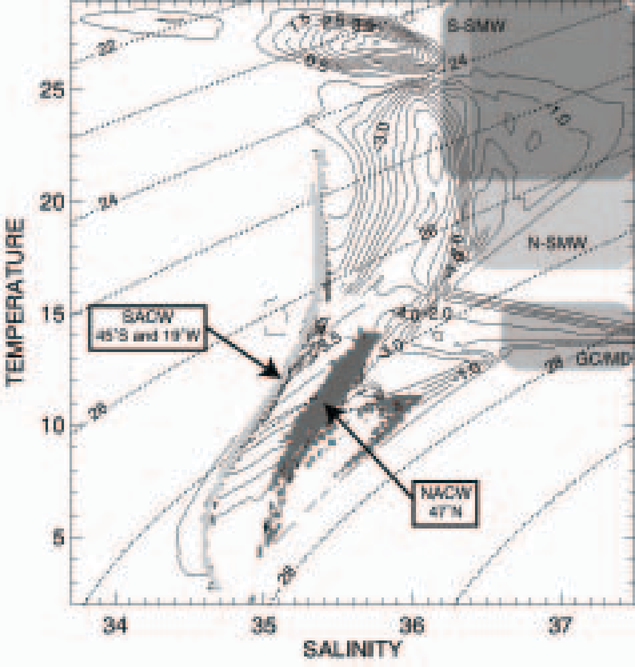

S-SMW
N-SMW
GCMD
SACW
45°S and 19°W
NACW
47°N
TEMPERATURE
SALINITY